Scientific Research Associates, inc.

50 Nye Road, P.O. Box 1058
Glastonbury, Connecticut 06033
(203) 659-0333

REPORT R88-920029-F

COMPUTATION OF FLOW AROUND MANEUVERING SUBMERGED BODIES

T.R. Govindan, W.R. Briley and R. Levy

Scientific Research Associates, Inc.
Glastonbury, CT 06033

Final Report
Contract N00167-86-C-0049

Prepared for:
Office of Naval Research
Department of the Navy
Arlington, VA 22217-5000

October 1988

Approved for Public Release; Distribution Unlimited

TABLE OF CONTENTS

ABSTRACT

Generalized primary/secondary flow equations and a spatial-marching solution algorithm have been utilized to develop a procedure to compute the three-dimensional viscous flow around a submerged body in maneuver. The primary/secondary flow equations are an approximation to the Navier-Stokes equations for flows in which a primary flow direction can be identified. Important elements of the approximation are a locally specified primary flow direction and a decomposition of the secondary velocity field to identify a small velocity vector for approximation. No approximations are introduced for pressure in this approach. The primary/secondary flow equations are a well-posed initial-value problem in a spatial coordinate nominally aligned with the primary flow direction and are solved by a sequentially decoupled implicit algorithm. The procedure provides an order to two orders-of-magnitude run time advantage over solution of the Navier-Stokes equations. Results are presented for the flow past an unappended submarine hull in drift at a Reynolds number of 16 million and incidence of 20 degrees. These results are consistent with experimental observations and provide a means to compute the complex three-dimensional viscous flow field economically.

1. INTRODUCTION

The flow around submerged bodies at different attitudes evokes considerable interest in the field of hydrodynamics. Such flow fields occur in many and varied applications. Of particular interest is the flow field around a submarine, torpedo, or similar body in maneuver. The computation of this flow field is important to the analysis of performance and noise characteristics of the device.

The flow field around a submerged body in maneuver is, in general, three-dimensional, viscous, and unsteady. The large scale unsteadiness in the flow field is primarily due to the time-dependent motion of the maneuvering body. The computation of this unsteady, three-dimensional, viscous flow field with available computer resources is a formidable task. However, many portions of a maneuver can be steady (e.g. a steady descent or climb) or quasi-steady, and the flow field around the body can be obtained from solution of the steady flow equations for a fixed body attitude. Several different attitudes can be studied in this manner. The results would provide body surface pressures which can then be used to derive the forces and moments on the body. The computation of this quasi-steady flow field is addressed in this report.

The complexity of the flow around a submerged body in steady maneuver presents considerable difficulties in the utilization of computational methods to compute such flows. These difficulties arise from the three-dimensionality of the flow field characterized by large secondary vorticity and velocity generated that result in a flow field with diverse length scale flow structures. Solution of the three-dimensional averaged Navier-Stokes equations avoids making physical approximations other than those associated with turbulence modeling. However, this approach is very costly, even with modern supercomputers, because the accurate resolution of the complex flow structures requires very large mesh densities. In light of this high cost of solution, approximations have been developed which reduce the steady subsonic Navier-Stokes equations to a form which is well-posed as an initial-value problem in a suitable direction and could be solved by a spatial-marching algorithm. The advantage of such an approach is that spatial-marching algorithms can be devised which are considerably less expensive in terms of computer resources (run time and storage) than algorithms for the elliptic Navier-Stokes equations. The trade-offs for this advantage are that errors are

introduced due to the approximations and the range of flow problems that can be addressed is restricted relative to the Navier-Stokes equations because of factors such as flow separation, stagnation points, and transonic flow effects. Nevertheless, this approach seems well suited for a number of flows arising in practical applications and can provide very high resolution of three-dimensional viscous flow structures at relatively low cost. In addition, the spatial-marching approach could provide a large number of detailed flow calculations at moderate cost for use in design optimization studies.

The potential gain in economy of solution for a class of complex three-dimensional viscous flows by utilizing a spatial-marching approach provided ample motivation to study and establish the applicability of the approach to compute the flow field around a submerged body in maneuver. This study of the applicability of the spatial-marching approach to compute the flow field around a submerged body was the primary focus of the present contract. Three aspects were identified and comprised the study:

(a) Establishment of a framework of approximations and governing equations suitable for the three-dimensional viscous flow around a submerged body in maneuver. The guiding principle in this process was that the approximations be valid considering the physics of the flow field and the governing equations be a well-posed initial value problem considering mathematical requirements for successful application of a spatial-marching solution algorithm.

(b) Formulation of governing equations for efficient numerical solution. Identification and application of efficient numerical solution procedures to achieve the run time advantages desired.

(c) Computation of the three-dimensional viscous flow around a submerged body to demonstrate successful completion of (a) and (b) and establish the applicability of the approach to compute the submerged body flow field.

All three aspects were successfully addressed under the present contract.

The next section of this report describes the generalized primary/secondary flow equations utilized as the approximate flow equations for the submerged body flow field and the sequentially decoupled implicit algorithm utilized to solve the equations efficiently. Application of the procedure to compute flow around a submerged body in maneuver is also described. The third section of the report describes results of the computations of the flow around a submerged body in drift and compares the results with available experimental

data. The report concludes with a description of current capability and suggestions for future development of the capability.

2. PHYSICAL APPROXIMATIONS AND GOVERNING EQUATIONS

2.1 Overview

Two basic types of physical/mathematical approximations have been suggested to reduce the Navier-Stokes equations to a form suitable for spatial-marching solution. Approximations in both viscous and inviscid terms in the Navier-Stokes equations are necessary to obtain non-elliptic (well-posed) approximate equations. The viscous approximation entails neglecting terms representing streamwise diffusion. This approximation requires identifying a direction in the flow field along which the approximation is made and associating the streamwise (marching) coordinate with this direction. Two types of inviscid approximations have been suggested: (a) an assumed form for the steamwise pressure gradient term, and (b) a small scalar potential approximation for the secondary flow. Either of these inviscid approximations, along with the viscous approximation, produces non-elliptic governing equations.

The inviscid approximation which assumes a given form for the streamwise pressure gradient term has obvious roots in two-dimensional boundary layer theory, and has been used extensively. The second type of inviscid approximation (termed the small scalar-potential approximation) has been investigated recently by Briley and McDonald [1]. This approximation does not employ any approximation for pressure gradient terms and instead approximates convective terms in the secondary flow momentum equation by neglecting the scalar-potential component of a vector-decomposed secondary-flow velocity field. The effect of the generated streamwise vorticity (secondary flow) on the pressure field is retained in the streamwise pressure gradient with the small scalar-potential approximation. This effect is usually absent in the streamwise pressure gradient when it is assumed to be of given form.

The inviscid and viscous approximations just described should not be confused with other equations under the general heading of 'parabolized Navier-Stokes' equations which are not well-posed initial-value problems but are solved iteratively by approximate well-posed spatial marching iterations. The iterations, when converged, remove the approximation made in each of the iterates to obtain solutions of the elliptic set of approximate flow equations.

Preliminary computations of the steady flow around a submerged body in drift with a spatial marching procedure were completed by Govindan and Levy [2]. These computations approximated streamwise pressure gradients in the governing equations by setting them to zero. At this level of approximation, the results demonstrated that the qualitative features of the three-dimensional viscous flow around a submerged body could be computed within the context of a spatial marching algorithm. These results provided a basis to further pursue and refine the approach to provide quantitatively accurate computations of the submerged body flow field, the objective of the present contract.

The first task addressed, under the present effort, was to develop the framework of approximations and governing equations suitable for the submerged body flow field. Govindan, Briley, and McDonald [3,4] have recently derived generalized primary/secondary flow equations as an approximate set of flow equations applicable to a wide class of three-dimensional viscous flows. These equations are an approximation of the steady Navier-Stokes equations based on knowledge of a primary flow direction which includes the effect of surface geometry. The primary/secondary flow equations along with the small scalar potential approximation are a well-posed initial value problem suitable for solution by a spatial marching algorithm. These equations were deemed to be the preferable set of equations for computing the flow around a submerged body in manuever for two reasons. First, Govindan, Briley and McDonald [4] in their computations have demonstrated the quantitative accuracy that could be obtained from the primary/secondary flow equations. Second, the choice of a potential flow model to generate streamwise pressure gradients for the pressure approximation is unclear and, therefore, the approximation is difficult to use. The difficulty does not arise with the small scalar potential approximation wherein no approximations are made for the streamwise pressure gradient.

2.2 Primary/secondary flow equations for the submerged body flow field

The physical approximations made in the primary/secondary flow equations are a distinguishing feature of the present approach. The present approximations are similar in spirit to those made in two-dimensional slender channel theory, and to a lesser degree in two- and three-dimensional boundary layers. In these latter approaches, one velocity component (the surface- or coordinate-normal component) is assumed to be small. In applications such

as flow about a submerged body, however, large steamwise vorticity is generated. The velocity components associated with this streamwise vorticity are known to be large (of the order of the streamwise velocity) and cannot be neglected. In the present approach, a small velocity vector is identified which provides a basis for approximating flows with large streamwise vorticity and secondary velocity.

Two features of the primary/secondary flow equations central to identifying a small velocity component for approximation are a locally specified primary-flow direction and a decomposition of the secondary velocity field. The local flow field velocity vector is expressed as a primary flow component in the primary-flow direction and a secondary flow component normal to this direction. The secondary velocity component is decomposed into components defined from a scalar-potential and a vector-potential. The vector potential defines the streamwise vorticity and the large secondary velocity component associated with the streamwise vorticity. The remaining scalar-potential velocity component contribution can be assumed to be small in the transverse momentum equations, but not otherwise neglected. This small scalar-potential approximation along with the viscous approximation neglecting streamwise diffusion is sufficient to establish a well-posed initial value problem, which can be solved far more economically than the Navier-Stokes equations. No approximations are introduced for pressure in this approach.

Figure 1 illustrates elements of the velocity decomposition and approximation. Figure 1a is a schematic showing a local primary flow direction and a plane normal to the direction (local normal plane). The flow field velocity vector is represented as a primary flow (streamwise) velocity component u_p in the primary flow direction and a secondary flow velocity vector $\vec{V}$ in the local normal plane. The primary flow direction does not, in general, coincide with the marching coordinate direction and correspondingly the local normal plane does not coincide with the transverse coordinate plane that is normal to the marching coordinate. The secondary flow velocity vector $\vec{V}$ is decomposed (Figure 1b) in the local normal plane into a component from a scalar-potential ($\vec{V}_\phi$) and a component from a vector potential ($\vec{V}_\psi$). The vector potential component $\vec{V}_\psi$ is associated with streamwise vorticity and is expected to be large. The scalar potential component $\vec{V}_\phi$ is the difference between the total velocity component $\vec{V}$ and $\vec{V}_\psi$ and is expected

to be small. The small scalar-potential approximation neglects the effects of $\vec{V}_\phi$ in transverse momentum equations. This component is not neglected in the continuity equation. A physical interpretation of the approximation for a general three-dimensional viscous flow field is not easy. However, the approximate equations can be reduced to two-dimensional boundary layer and slender channel theory equations. In this boundary layer context, the scalar-potential component $\vec{V}_\phi$ corresponds to the small velocity component normal to the boundary.

An important element in the application of the primary/secondary flow equations to compute three-dimensional viscous flow is to identify a local primary flow direction. Potential flow streamlines conform to the shape of boundaries and are a suitable choice for the primary flow direction for many flow problems. In the case of the submerged body flow field, the primary flow direction was chosen to be direction of potential flow streamlines around the body at zero incidence. This potential flow was calculated using slender body theory [5].

Validation of the spatial-marching approach requires comparison of the computation with experimental measurements and other computational results. In Ref. [4], computed velocities for both laminar and turbulent flow in a 90-degree square bend agree very well with measurements of Taylor, Whitelaw, and Yianneskis [6]. A comparison with a Navier-Stokes solution for a 90-degree channel bend gives excellent agreement with both pressure and velocity [4]. In Ref. [7], surface pressures computed for a tip vortex flow field are in good agreement with measurements of Gray, McMahon, Shenoy and Hammer [8]. In the present study, the flow past an unappended submarine hull in drift has been computed at a Reynolds number of 16 million and incidence of 20 degrees.

The remainder of this section contains a mathematical description of the generalized primary/secondary flow equations and the small scalar-potential approximation. Details of the derivation of these equations can be found in Ref. [3]. In the summary that follows, $\bar{i}_k$ denotes the unit vector basis associated with the orthogonal reference line coordinate system used to describe the equations. The vector $\bar{i}_1$ is aligned with the marching coordinate direction (x_1) and vectors $\bar{i}_2$ and $\bar{i}_3$ lie in the transverse coordinate plane. The vector basis $\bar{e}_k$ and the reciprocal basis $\bar{e}^k$ are

defined to identify the local primary flow direction and the local normal plane for the purpose of approximating flow equations. The vector $\bar{e}^1$ is aligned with the primary flow direction and the vectors $\bar{e}^2$ and $\bar{e}^3$ lie in the local normal plane [Figure 1.a.]. The vectors $\bar{e}^k$ and $\bar{e}_k$ are related and can be written in terms of their components in the coordinate system $\bar{i}_k$ as

$$\bar{e}_k \cdot \bar{e}^{\ell} = e_{km} e^{m\ell} = \delta_k^{\ell} \tag{2.1}$$

The flow field velocity vector is denoted by $\bar{U}$,

$$\bar{U} = u_1 \bar{i}_1 + u_2 \bar{i}_2 + u_3 \bar{i}_3 = u_p \bar{e}^1 + v\bar{e}^2 + w\bar{e}^3 \tag{2.2}$$

The velocity component u_p is associated with the primary flow direction and components v and w with the secondary flow field. The secondary flow velocity vector $\bar{V}$ can be defined as

$$\bar{V} = v\bar{e}^2 + w\bar{e}^3 \tag{2.3}$$

The secondary flow velocity components are decomposed into scalar potential (v_ϕ, w_ϕ) and vector potential components (v_ψ, w_ψ)

$$\begin{aligned} v &= v_\phi + v_\psi \\ w &= w_\phi + w_\psi \\ \bar{V} &= \bar{V}_\phi + \bar{V}_\psi \end{aligned} \tag{2.4}$$

The scalar potential velocity components can be defined in terms of a scalar potential (ϕ) and the vector potential components in terms of a vector potential (ψ).

$$\nabla_s\phi = (e^{\ell j}\bar{V}_\phi\cdot\bar{e}_j)\bar{i}_\ell$$

$$\ell = 2,3 \text{ (no sum)} \qquad (2.5)$$

$$\nabla_s\times\psi\bar{i}_1 = (\rho e^{\ell j}\bar{V}_\psi\cdot\bar{e}_j)\bar{i}_\ell$$

where ρ is density and ∇_s is the surface operator defined as

$$\nabla_s = \nabla - \nabla_p \qquad (2.6)$$

with $$\nabla_p = \bar{i}_1(\bar{i}_1\cdot\nabla)$$

All variables in the flow equations are assumed to be nondimensional, having been normalized by a suitable combination of reference quantities. The primary/secondary flow equations are written for the dependent variables, streamwise velocity u_p, scalar potential ϕ, vector potential ψ, vorticity Ω, pressure p, total enthalpy E, and density ρ.

Scalar potential equation (continuity):

$$\nabla_s\cdot(\rho\nabla_s\phi) + \nabla_p\cdot(\rho e^{1j}\bar{V}\cdot\bar{e}_j)\bar{i}_1 + \nabla\cdot(\rho e^{kl}u_p)\bar{i}_k = 0 \qquad (2.7)$$

Streamwise momentum equation:

$$\rho\bar{U}\cdot\nabla u_p - \rho\bar{U}\cdot(\bar{U}\cdot\nabla)\bar{e}_1 + \bar{e}_1\cdot\nabla p + \frac{1}{Re}\bar{e}_1\cdot\bar{\nabla}\times\mu\bar{\nabla}\times\bar{U} = 0 \qquad (2.8)$$

where Re is the Reynolds number defined from reference quantities, μ the normalized coefficient of molecular viscosity, and $\bar{\nabla}$ is an approximation to ∇ in which second derivatives along the $\bar{i}_1$ coordinate have been neglected.

Vector potential equation (definition of vorticity):

$$\nabla_s\times\frac{1}{\rho}(\nabla_s\times\psi\bar{i}_1) - \Omega\bar{i}_1 = 0 \qquad (2.9)$$

Vorticity transport equation:

$$\frac{\rho u_p}{h}\frac{\partial \Omega}{\partial x_1} + \nabla_s\cdot\rho\bar{V}\bar{\Omega} + \nabla_s\times(e^{\ell k}C_k - D^{\ell})\bar{i}_\ell + (\nabla_s\frac{\rho u_p}{h})\times\frac{\partial e^{\ell k}}{\partial x_1}(\bar{V}\cdot\bar{e}_k)\bar{i}_\ell$$

$$+ (\nabla_s\rho\bar{V})\times[\nabla_s e^{\ell k}(\bar{V}\cdot\bar{e}_k)]\bar{i}_\ell + \frac{1}{Re}\nabla_s\times e^{\ell k}\bar{e}_k\cdot\nabla_s\times\mu\Omega\bar{i}_1 = 0 \qquad (2.10)$$

where C_k and D^{ℓ} are defined in [3] and $\bar{V} = \beta\bar{V}_\phi + \bar{V}_\psi$. The parameter β takes on values of 0 or 1, $\beta = 0$ identifies the small scalar potential approximation.

Pressure equation:

$$\nabla_s\cdot(e^{\ell k}\bar{e}_k\cdot\nabla p)\bar{i}_\ell + \nabla_s\cdot(e^{\ell k}F_k)\bar{i}_\ell = 0 \quad \ell = 2,3 \text{ (no sum)} \qquad (2.11)$$

F_k is a combination of terms from transverse momentum equations and is defined in [3]. The secondary flow velocity vector, $\bar{V}$, is written as $\bar{V} = \beta\bar{V}_\phi + \bar{V}_\psi$ in F_k and $\beta = 0$ identifies the small scalar potential approximation.

Energy equation:

$$\rho\bar{U}\cdot\nabla E - (RePr)^{-1}\nabla\cdot\kappa\nabla_s E - (\gamma-1)M_r^2Re^{-1}[\mu\Phi - \rho\bar{U}\cdot\nabla_s\times\mu\nabla_s\times\bar{q}$$

$$- Pr^{-1}\nabla_s\kappa\nabla_s|\bar{q}|^2/2] = 0 \qquad (2.12)$$

where $\bar{q} = u_p\bar{e}^1 + (\beta v_\phi + v_\psi)\bar{e}^2 + (\beta w_\phi + w_\psi)\bar{e}^3$,

Φ is the dissipation function, κ the coefficient of thermal conductivity, Pr the Prandtl number, and M_r the reference Mach number. Simpler forms of the energy equation that can be used at low and moderate Mach numbers are described in [3].

State equation:

$$p = \rho E/\gamma M_r^2 - (\gamma-1)\rho|\bar{q}|^2/2\gamma \qquad (2.13)$$

Equations (2.7) to (2.13), along with the definition of the velocity decomposition (2.5), are the complete set of primary/secondary flow equations. The small scalar potential approximation ($\beta = 0$) makes these equations a well-posed initial value problem along the streamwise coordinate (x_1).

3. SOLUTION OF PRIMARY/SECONDARY FLOW EQUATIONS

The choice of a solution algorithm for the primary/secondary flow equations must exploit the small scalar potential approximation for economy. The potential for economy lies in the initial-value nature of the primary/secondary flow equations and the ability to solve such a problem by a spatial marching scheme. Such a scheme will be developed in this section for the primary/secondary flow equations.

An evolution equation can be written in the form

$$A \frac{\partial \phi}{\partial t} + D(\phi) = 0 \qquad (3.1)$$

where ϕ is a vector of dependent variables, t is a time-like variable (e.g. streamwise coordinate), A is a matrix of coefficients, and D is a multi-dimensional differential operator. Efficient, implicit, noniterative marching schemes have been developed to solve equations of the type (3.1) when the matrix A is well-conditioned. An example of such a scheme is the LBI scheme [9] for nonlinear equations and is based on the Douglas-Gunn ADI scheme. However, the matrix A for the primary/secondary flow equations is singular due to the lack of streamwise derivatives in some of the governing equations. This is also true when the same equations are written in terms of primitive variables [3]. Coupled implicit schemes such as the LBI scheme require iteration when A is singular. This penalty in economy, due to iteration of a fully coupled system at each step, is avoided in the present sequentially decoupled algorithm.

The problem with the singularity of the coefficient matrix of the streamwise derivative is circumvented by decoupling the individual equations of the system without a streamwise derivative and solving them separately at each streamwise step of a spatial marching scheme for the remaining equations. However, any severe penalty in economy due to loss of stability in the overall scheme from the decoupling would be unacceptable. The present sequentially

decoupled implicit algorithm decouples the primary/secondary flow equations into subsystems through sequencing and linearization of the subsystems. Each of the subsystems can then be solved by economical, stable, implicit procedures.

3.1 Sequentially Decoupled Implicit Algorithm

The solution algorithm for the primary/secondary flow equations is developed by considering a more general case of a partial differential equation in the form

$$Mq = 0 \tag{3.2}$$

M is a matrix operator (nonlinear) whose elements are the coefficients and differential operators of the individual equations of the system and q is a vector of dependent variables. Further, the elements of q are assumed to be ordered and the sequence of equations in M arranged on the basis of an association between an equation and a dependent variable. This association between individual equations of the system and dependent variables will be clarified with development of the algorithm. The matrix M is decomposed and (3.2) written in the form

$$(L + D + U)q = 0 \tag{3.3}$$

where L, D, U are matrix operators containing the lower diagonal, diagonal and upper diagonal elements of M, respectively. The matrix operators L, D and U are linearized by the following linearization scheme

$$L^{n,n+1} : \ell_{ij}\,(q_k^{n+1},\ q_m^{n}) \qquad \begin{matrix} k = 1, \ldots (j-1) \\ m = j, \ldots N \end{matrix} \tag{3.4}$$

where ℓ_{ij} are the elements of L and n is the marching coordinate index. The operators D and U can be linearized in the same manner as L. Equation (3.3) can be written as a linear, decoupled set of equations

$$(D^{n,n+1} + L^{n,n+1})\ q^{n+1} + U^{n,n+1}\ q^{n} = 0 \tag{3.5}$$

or

$$D^{n,n+1}\, q^{n+1} = -\left(L^{n,n+1}\, q^{n+1} + U^{n,n+1}\, q^{n}\right) \tag{3.6}$$

Equation (3.6) is a decoupled system of equations that can be solved by inverting the linear diagonal operators in sequence using implicit schemes. Clearly, the success of the sequentially decoupled algorithm (3.6) depends on the system of equations (3.2) and the choice of the diagonal matrix operator, D. The diagonal operator, D, is determined by the association made between individual equations of the system and dependent variables.

The association of equations with variables is straightforward for the primary/secondary flow equation; Ω with (2.10), ψ with (2.9), p with (2.11), u_p with (2.8), ϕ with (2.7), and E with (2.12). For simplicity, the implicit operator $(D^{n,n+1} + L^{n,n+1})$ in (3.5) for the incompressible form of the primary/secondary flow equations can be written as

$$(D^{n,n+1} + L^{n,n+1})\, q^{n+1}$$

$$= \begin{bmatrix} d_{11} & * & & * & \\ 1 & \nabla_s^2 & & & \\ \ell_{31} & \ell_{32} & \nabla_s^2 & * & * \\ 0 & 0 & \frac{1}{h}\frac{\partial}{\partial x} & d_{44} & \\ 0 & 0 & 0 & \frac{\partial}{\partial x} & \nabla_s^2 \end{bmatrix} \begin{bmatrix} \Omega \\ \psi \\ p \\ u_p \\ \phi \end{bmatrix}^{n+1} \tag{3.7}$$

where d_{11}, $d_{44} = U\cdot\nabla - Re^{-1}\nabla_s^2$. The '*' in (3.7) is used to indicate non-zero elements of the explicit operator, $U^{n,n+1}$. The vector basis is assumed aligned with coordinate directions in (3.7). The vector basis introduces more complex differential operators in individual equations but the implicit operator retains essentially the same form as (3.7). Although no stability analysis of (3.6) has been performed, stability of (3.6) for the primary/secondary flow

equations has been established through extensive numerical computation of numerous test cases. Further, although the vorticity and vector potential equations (first two equations in (3.7)) can be uncoupled in (3.7), they are strongly coupled at a no-slip boundary by boundary conditions. Consequently, the vorticity and vector potential equations are solved as a coupled subsystem of equations to avoid stability problems. The following sequentially decoupled subsystem equations are obtained for the compressible primary/secondary flow equations

1) vorticity (2.10), vector potential (2.9) for Ω, ψ
2) pressure equation (2.11) for p
3) energy equation (2.12) for E
4) streamwise momentum (2.8) for u_p
5) equation of state (2.13) for ρ (algebraic)
6) scalar potential equation (2.7) for ϕ

The sequence completes the solution of the primary/secondary flow equations for one streamwise step (n+1) from the solution at the previously computed step (n) (initial conditions for n=1). Each of the individual subsystem equations can be solved by a convenient, efficient procedure. Numerical procedures used in the present work for solving decoupled subsystem equations are described in a later section.

3.2 Differencing Procedures and Boundary Conditions

The governing equations (2.7)-(2.12) are transformed to a body-fitted coordinate system in which the equations are discretized. Body-fitted coordinate transformations suitable for the primary/secondary flow equations are discussed in [3]. The discretization employs two-point backward differences for streamwise derivatives and three-point central differences for transverse derivatives. The body-fitted coordinate transformation allows a variable streamwise step size and concentration of grid points in regions of expected large gradients. A centered Crank-Nicolson formulation could be used for streamwise derivatives but the formal accuracy of the scheme would not be improved because of the first-order accurate linearization scheme (3.4) used to decouple subsystem equations.

Implicit boundary conditions are used in all subsystem equations. Boundary conditions that are not straightforward are no-slip conditions on a solid boundary and boundary conditions on pressure. These conditions are described here. The streamwise velocity u_p is specified as zero in the streamwise momentum equation (2.8) on a no-slip boundary. The condition $v = w = 0$ must be expressed in terms of ϕ, ψ and Ω. The normal component of the scalar potential velocity is specified as zero by $\bar{i}_n \cdot \bar{V}_\phi = 0$, where $\bar{i}_n$ is the unit normal vector to the boundary. V_ϕ is specified in terms of ϕ to obtain a Neumann condition for the scalar potential equation (2.7). The normal component of the vector potential velocity is specified zero by prescribing $\psi = 0$ on the boundary. The tangential component of the transverse velocity is specified at the no-slip boundary by

$$\bar{i}_t \cdot [(v_\phi + v_\psi)\bar{e}^2 + (w_\phi + w_\psi)\bar{e}^3] = 0 \qquad (3.8)$$

where $\bar{i}_t$ is the unit tangent vector to the boundary. Equation (3.8) combined with equation (2.9) is used to obtain Ω on the boundary in terms of ϕ and ψ. This relation for Ω, along with prescribing $\psi = 0$, provides coupled boundary conditions for the vector potential (2.9) and vorticity equations (2.10). The coupled boundary conditions require the equations to be solved as a coupled subsystem from stability considerations.

Boundary conditions for pressure are obtained by computing the normal gradient of pressure on the boundary from transverse momentum equations. The prescription of the normal gradient of pressure in the pressure equation (2.11) results in a Neumann problem. Solution of the Neumann problem leaves an undetermined constant in the transverse plane that could, however, be a function of the streamwise coordinate. Pressure, p, is written as

$$p = p_m(x_1) + p_v(x_1, x_2, x_3) \qquad (3.9)$$

where p_m is the undetermined constant of the Neumann problem and p_v is the solution of the pressure equation. The value of p_m is required in the solution of the streamwise momentum equation (2.8) in the form of the streamwise gradient, $\frac{\partial p_m}{\partial x_1}$. In external flows, p_m can be determined by equating

the right-hand side of (3.9) to prescribed pressure at a point in freestream in each transverse plane. Such a condition is not available in internal flows and p_m has to be determined to ensure that the integral mass flux relation

$$\int_A \rho \bar{U} \cdot \bar{i}_1 \, dA = Q = \text{constant} \tag{3.10}$$

is satisfied. For internal flows, p_m is adjusted by a secant iteration during solution of the streamwise momentum equation (2.8) so that integral mass flux relation (3.10) is satisfied.

Far field boundary conditions for velocity for the submerged body flow field are specified in terms of freestream conditions and the angle of attack. The streamwise velocity and vorticity are extrapolated at the outer boundary. The vector potential component of the transverse velocity field is specified in terms of the angle of attack (α) as

$$\bar{i}_2 \cdot \nabla_s \times \psi \bar{i}_1 = U_\infty \sin\alpha \tag{3.11}$$

Equation (3.11) is integrated along the outer boundary for a specification of ψ. The scalar potential component of the transverse velocity is specified in terms of the normal gradient of the scalar potential

$$\bar{i}_n \cdot \nabla_s \phi = -\sum_j \frac{Q_j}{2\pi} \bar{i}_n \cdot \left\{ \frac{\bar{r}}{r^2} + \frac{\bar{r}_i}{r_i^2} + \frac{\bar{r}_0}{r_0^2} \right\} \delta x_2 \delta x_3 \tag{3.12}$$

where $\bar{r}$ is the vector from the grid point j to the boundary point under consideration, $\bar{r}_i$ is the vector from the image of the grid point j to the boundary point, and $\bar{r}_0$ is the vector from the origin to the boundary point. Q_j is the source strength obtained from (2.7) as

$$Q_j = \nabla_p \cdot (\rho e^{1j} \bar{v} \cdot \bar{e}_j) \bar{i}_1 + \nabla \cdot (\rho e^{kl} u_p) \bar{i}_k \tag{3.13}$$

The summation in (3.12) is carried out over all grid points in the transverse plane, extending 2π around the body.

3.3 Turbulence Model

The mixing length turbulence model developed by Baldwin and Lomax [10] was utilized to compute the eddy viscosity. In utilizing the model for the submerged body flow field, problems were encountered in the computation of the vorticity function (FMAX). In the region of the lee-side vortex, a second peak in the vorticity function was found near the center of the vortex. This peak was of greater value than the first peak found in the boundary layer region of the flow field. If the second peak was utilized in the model, large eddy viscosities were computed in the region of the lee-side vortex which is physically a region of rotational inviscid flow. Large eddy viscosities in the region of the vortex dissipated the vortex in the computations. To overcome the problem, the turbulence model was modified to restrict the search for the peak in the vorticity function to $y^+ = 2000$. Similar modifications to the mixing length model have been used in the computations of Degani and Schiff [11] and Panaras and Steger [12].

3.4 Summary

A summary of the procedure used to advance the solution a single streamwise step to the (n+1) level from previously computed quantities at the n level follows. Coordinate and vector basis information required to solve the primary/secondary equations are prescribed input. Governing equations are assumed to be linearized and discretized as previously described.

(1) Equations (2.9) and (2.10) form a linear coupled system for ψ^{n+1} and Ω^{n+1}, which is solved as a (2×2) coupled system. For this purpose, artificial time derivatives are added to each equation and an iterative block-implicit scheme [9] is used. In prescribing no-slip boundary conditions, the tangential component (3.8) contains a contribution from ϕ; this contribution is evaluated using ϕ^n. Linearization (3.4) provides that terms involving other unknown dependent variables are evaluated at the n-level.

(2) The pressure equation (2.11) is solved for p_v^{n+1} using an iterative scalar ADI scheme. Updated values of v_ψ^{n+1} and w_ψ^{n+1} are available while other dependent variables are evaluated at the n-level.

(3) The energy equation (2.12) is solved for E^{n+1} using a scalar ADI scheme.

(4a) The streamwise momentum equation (2.8) is solved for u_p^{n+1} using a scalar ADI scheme. The streamwise pressure gradient is evaluated at the (n+1) level.

(4b) The density ρ^{n+1} is evaluated algebraically from the equation of state (2.13)

(5) Finally, the scalar potential equation (2.7) is solved for ϕ^{n+1} using an iterative scalar ADI scheme.

4. COMPUTED RESULTS FOR FLOW PAST A SUBMERGED BODY IN DRIFT

The primary focus of the present effort has been to demonstrate the capability to compute the three-dimensional viscous flow around an unappended submarine hull in drift, utilizing the generalized primary/secondary flow equations. Results of the computed flow field around an unappended submarine hull in drift (20 degrees) are presented here. These results are compared with the limited experimental data available for this flow case. The Reynolds number of the flow based on the length of the hull was 1.68×10^7. Computations were carried out for one-half of the symmetric flow field on a grid of 99 circumferential points, 70 radial points and 191 streamwise points (1.32×10^6 total grid points).

Figure 2 provides a visualization of the roll-up of the lee-side vortex through particle paths traced in the computed flow field. Particle traces are started in the upstream boundary layer at four streamwise stations. Figure 3 shows a contour plot of the streamwise velocity at several transverse planes. Figure 4 shows a similar contour plot of the computed static pressure

at several transverse planes. Figures 2-4 provide a basis for the description of the physical processes in the flow around the hull in drift. The cross flow component of the velocity field, due to drift of the hull, convects low momentum fluid in the boundary layer on the hull towards the lee side. This is clearly visible in the trajectories of the particle paths in the upstream flow (Figure 2). The low momentum fluid on the lee side rolls up into a vortex and is convected downstream by the streamwise velocity. The upstream static pressure distribution on the hull (Figure 4) shows a low pressure region (blue) on top of the hull caused by the acceleration of the cross flow velocity component. The pressure recovers on the lee side of the body. However, as the lee side vortex is generated, a low pressure region forms at the center of the vortex. The low pressure region in the vortex core significantly distorts the pressure field at the stern. The high pressure (red) region at the nose of the body is due to the stagnation point at the nose. The stagnation point is also the source of the streamwise velocity gradients at the nose (Figure 3). Figures 2 and 3 also show boundary layer fluid being convected away from the nose, on the lee side, along the symmetry plane. It is not yet clear whether this aspect of the flow field has been observed in experiments or is related to the initial velocity profiles assumed in the computations.

Figures 5 and 6 show vector plots of the transverse velocity field at two streamwise stations ($x = 0.8$ and 0.95). These plots provide a visualization of the structure of the lee side vortex. Transverse velocity vectors have been colored by the static pressure field, providing a relation between the transverse velocity and pressure fields. The plots clearly show the low pressure regions at the vortex center and on the hull. The pressure field also shows the interaction between the pressure field due to the vortex and the body pressure field. Figure 7 compares the computed transverse velocity field at $x = 0.95$ with measurements at $x = 1.0$. These measurements were provided by DTRC. The strength of the computed and measured vortices compare well with each other but the computed vortex is located closer to the body than in the measurements. The source of discrepancy in the location of the vortex could be due to modifications adopted in the turbulence model to compute the boundary layer length scale or due to inadequate resolution of the computed flow field in the stern region. Some of the discrepancy could also be attributed due to the different streamwise locations of the measurements and computations. The

computations were not carried out to x=1.0 due to the computational grid resolution being inadequate in this region, in the present case. Further, the measured lee side vortices are asymmetric. Means to include this effect in the computations were beyond the scope of the present effort.

Figure 8 shows the distribution of the computed axial and side forces on the hull. The figure shows the distribution of forces due to the pressure field alone and the distribution due to the total force (pressure and shear). The viscous shear stress does not alter the distribution of the force but does change the magnitude of the force slightly. As would be expected, the viscous shear stress affects the axial force to a greater magnitude than the side forces. Although the viscous shear stress does not significantly affect the side forces, the pressure field in itself is significantly altered by the viscous flow, as compared to potential flow, producing a net side force and axial force on the hull. The side force distribution on the hull (Figure 8) shows a positive force distribution at the nose which decreases beyond the nose. The side force increases again as the lee side vortex is generated. The side force is negative at the stern. The side force distribution produces a net positive force on the hull. The axial force distribution shows small regions of negative drag induced by the pressure field at the nose and stern of the hull. The axial force distribution produces a net positive drag on the hull, as would be expected.

5. CONCLUSIONS

The feasibility of computing the three-dimensional high Reynolds number flow around unappended hulls in drift using the generalized primary/secondary flow equations and the spatial marching computation procedure has been demonstrated. Important features of the flow field have been captured in the computations. The computations compare well, in terms of the vortex strength, with the limited experimental data available for the flow case. Computed forces on the hull show expected features. The computation procedure is very economical considering details of the flow field provided. The procedure typically requires 20 minutes of CRAY X-MP CPU time for 10^6 grid points.

6. FUTURE WORK

Computed flow field results need more detailed validation by comparison with experimental data to identify any sources of discrepancy in the computations. Determination of the length scale for use in the mixing length turbulence model for the three-dimensional viscous flow around the hull needs to be carefully evaluated. A two-equation turbulence model may be required in the computations. The computation procedure needs to be extended to include the effects of appendages on the hull. The spatial marching procedure could also be extended to include unsteady maneuvers. Such a procedure would still provide significant computational advantages over solution of the unsteady Navier-Stokes equations, especially for the long time scales involved in a maneuver and for low mach number flows. The present procedure could also be used as a tool to provide insight into the basic physical processes of asymmetric flows around the hull.

7. ACKNOWLEDGEMENTS

The authors would like to thank Drs. Ming-Shun Chang and Richard Curphey of DTRC for helpful discussions on the results of this study and Dr. F. de Jong for his suggestions during the course of this effort.

References

1. Briley, W.R. and McDonald, H.: Three-Dimensional Viscous Flow with Large Secondary Velocity, Journal of Fluid Mechanics, Vol. 144, pp. 47-77, 1984.

2. Govindan, T.R. and Levy, R.: Computation of Flow Around Maneuvering Submerged Bodies, GHR Program Final Report, Contract N00014-85-C-0253, September 1986.

3. Govindan, T.R., Briley, W.R. and McDonald, H.: Generalized Three-Dimensional Viscous Primary/Secondary Flow Equations for Internal and External Flows, Part I - Approximations and Formulation of Equations, SRA Report R87-1 (paper in preparation).

4. Govindan, T.R., Briley, W.R. and McDonald, H.: Generalized Three-Dimensional Viscous Primary/Secondary Flow Equations for Internal and External Flows, Part II - Numerical Solution and Results, Report R87-2 (paper in preparation).

5. Karamcheti, K.: Principles of Ideal-Fluid Aerodynamics, Robert E. Krieger Publishing Company, New York, 1980.

6. Taylor, A.M.K.P., Whitelaw, J.H. and Yianneskis, M.: Measurements of Laminar and Turbulent Flow in a Curved Duct with Thin Inlet Boundary Layers, NASA Contractor Report CR-3367, 1981.

7. De Jong, F.J., Govindan, T.R., Levy, R and Shamroth, S.J.: Validation of a Forward-Marching Procedure to Compute the Tip Vortex Generation Process for Ship Propeller Blades, presented at the 17th Symposium on Naval Hydrodynamics, The Hague, The Netherlands, 1988.

8. Gray, R.B., McMahon, H.M., Shenoy, K.R. and Hammer, M.L.: Surface Pressure Measurements at Two Tips of a Model Helicopter Rotor in Hover, NASA CR-3281, 1980.

References (Continued)

9. Briley, W.R. and McDonald, H.: On the Structure and Use of Linearized Block Implicit Schemes, J. Comp. Physics, Vol. 34, No. 1, pp. 54-72, January 1980.

10. Baldwin, B.S. and Lomax, H.: Thin-Layer Approximation and Algebraic Model for Separated Turbulent Flows, AIAA paper 78-257, 1978.

11. Degani, D. and Schiff, L.B.: Computation of Turbulent Supersonic Flows around Pointed Bodies Having Crossflow Separation, J. Comp. Phy., Vol. 66, No. 1, pp. 173-196, 1986.

12. Panaras, A.G. and Steger, J.L.: A Thin-Layer Navier-Stokes Solution of the Flow About a Prolate Spheroid, AGARD, AR-255, 1988.

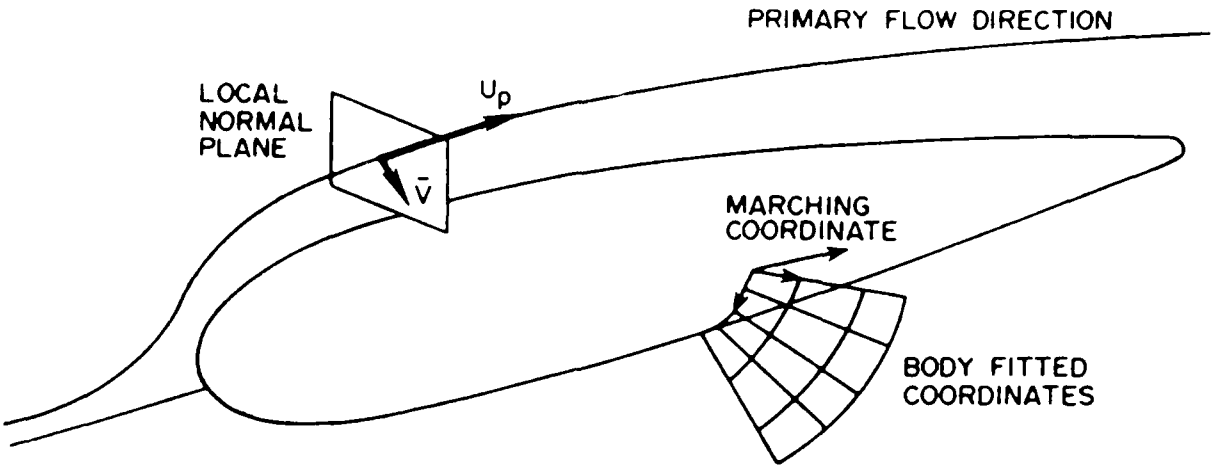

Figure 1a. Illustration of Primary Flow Direction.

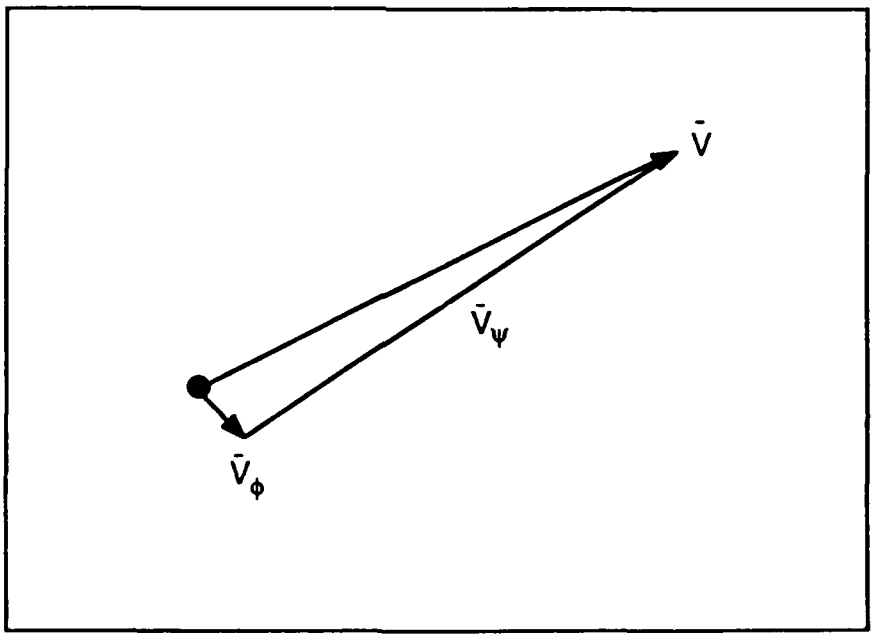

Figure 1b. Vector Decomposition of Transverse Velocity.

Figure Captions for Color Plates

Figure 2. Particle paths showing lee-side vortex roll-up.

Figure 3. Contour plot of streamwise velocity at several transverse planes.

Figure 4. Contour plot of static pressure at several transverse planes.

Figure 5. Vector plot of the transverse velocity field colored by static pressure ($x = 0.8$).

Figure 6. Vector plot of the transverse velocity field colored by static pressure ($x = 0.95$).

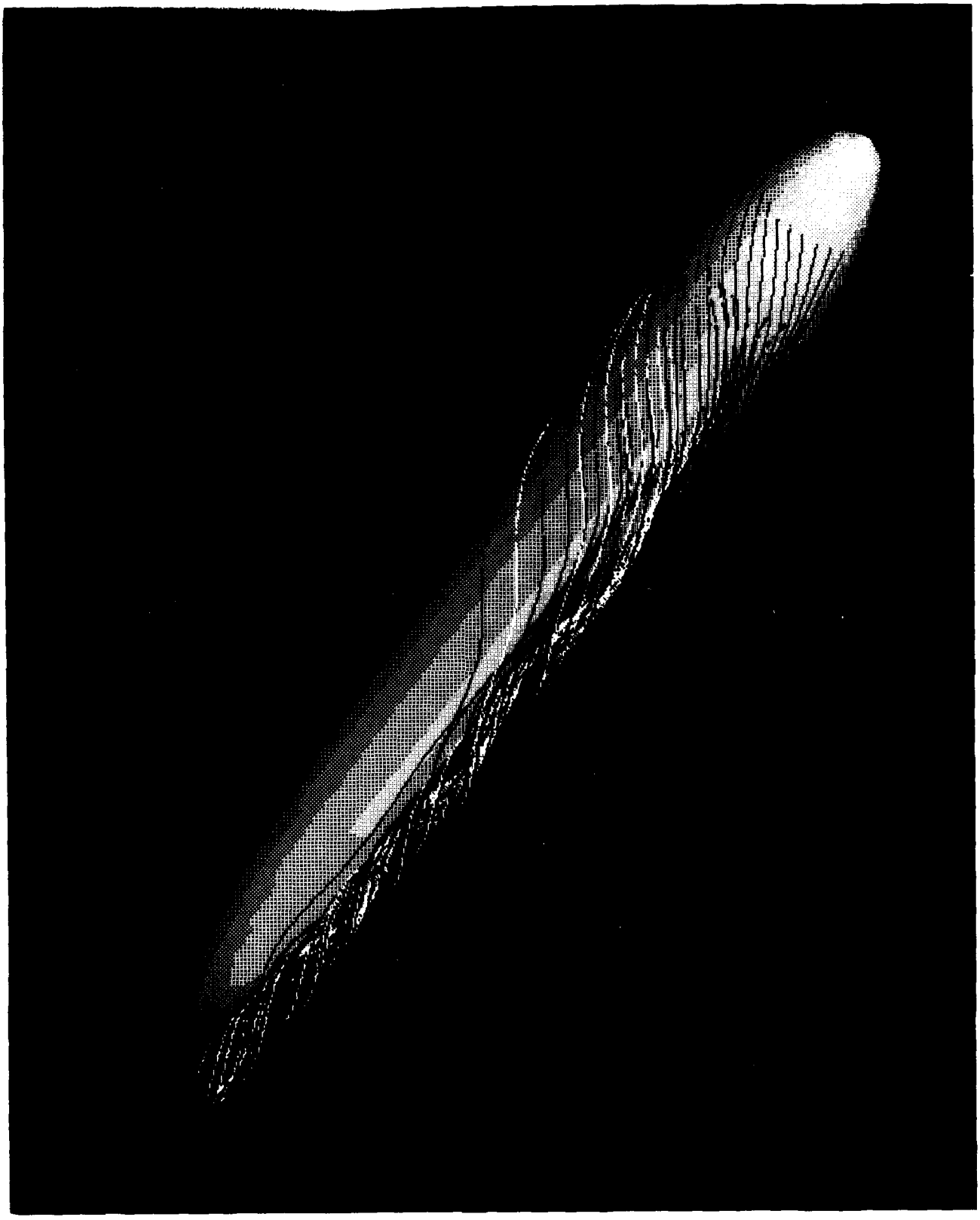

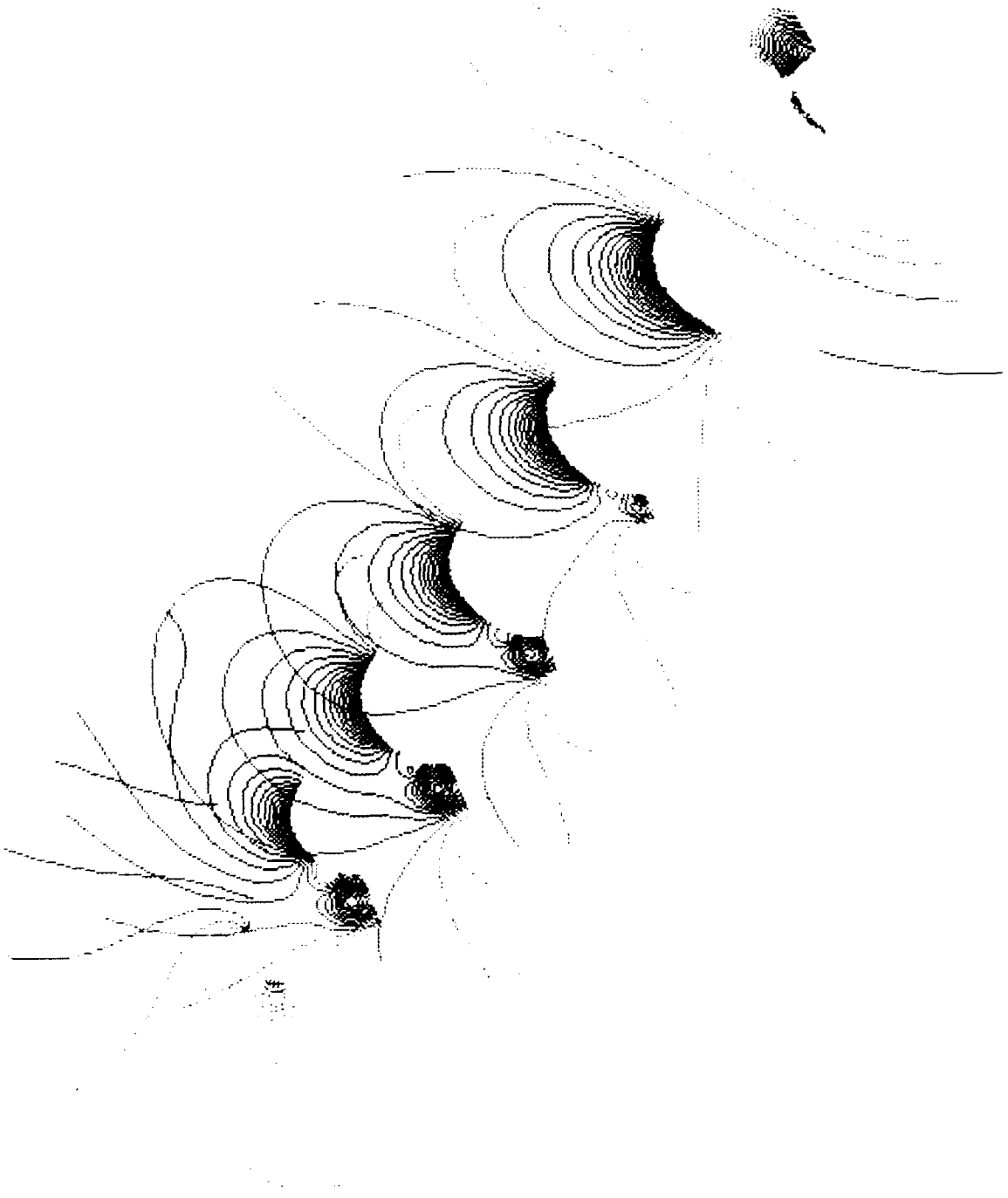

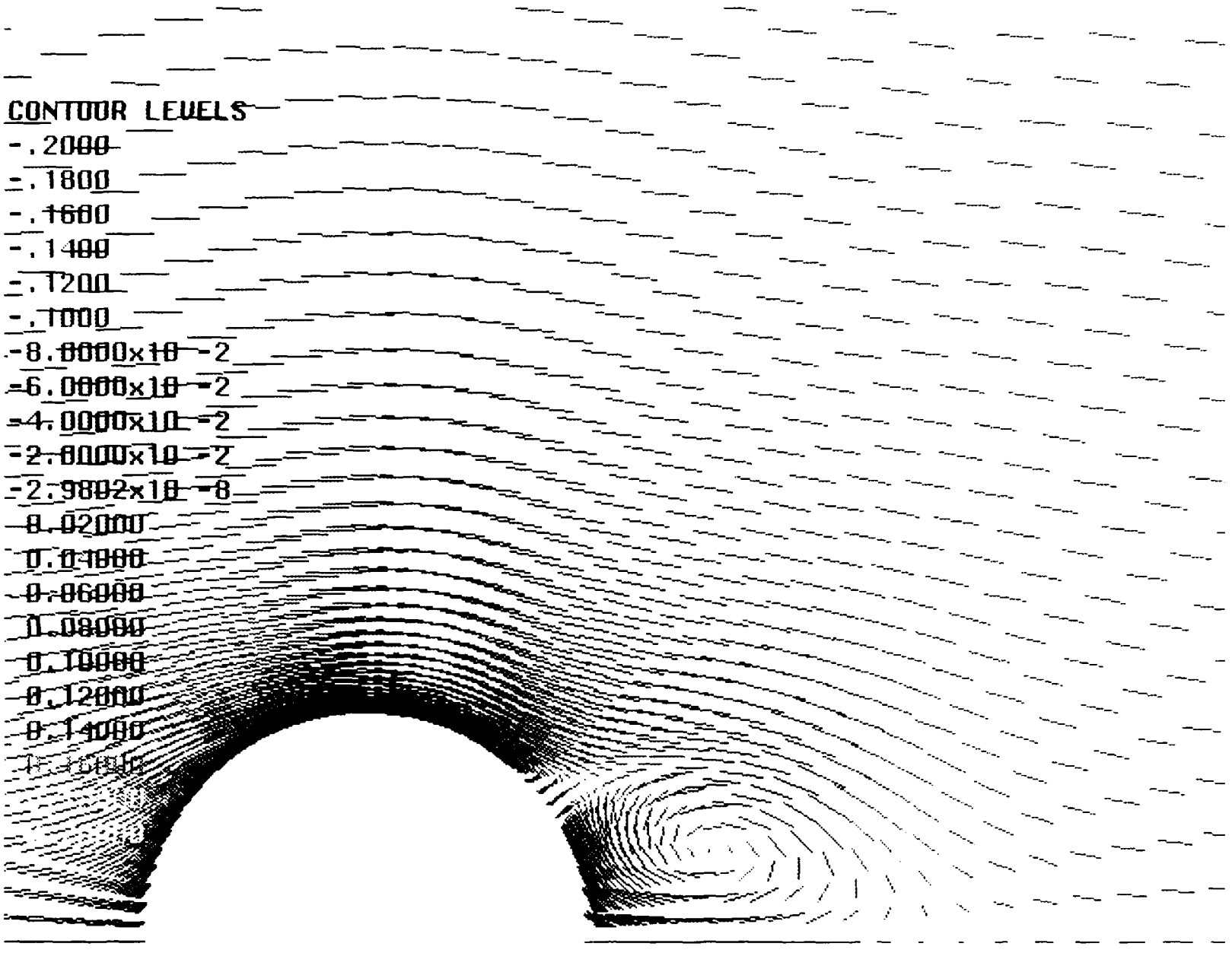
CONTOUR LEVELS
-.2000
-.1800
-.1600
-.1400
-.1200
-.1000
-8.0000x10 -2
-6.0000x10 -2
-4.0000x10 -2
-2.0000x10 -2
-2.9802x10 -8
0.02000
0.04000
0.06000
0.08000
0.10000
0.12000
0.14000

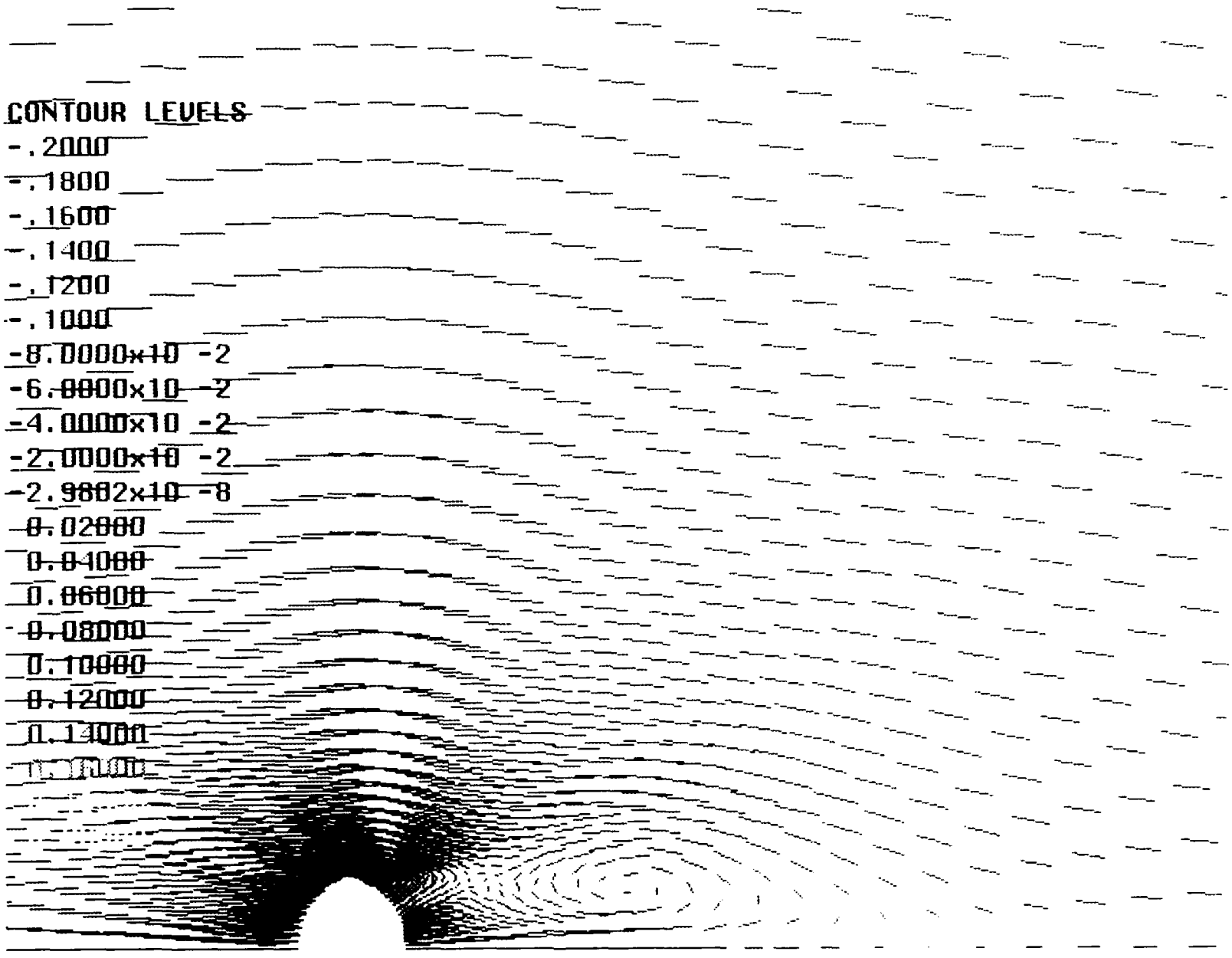
CONTOUR LEVELS
-.2000
-.1800
-.1600
-.1400
-.1200
-.1000
-8.0000x10 -2
-6.0000x10 -2
-4.0000x10 -2
-2.0000x10 -2
-2.9802x10 -8
0.02000
0.04000
0.06000
0.08000
0.10000
0.12000
0.14000

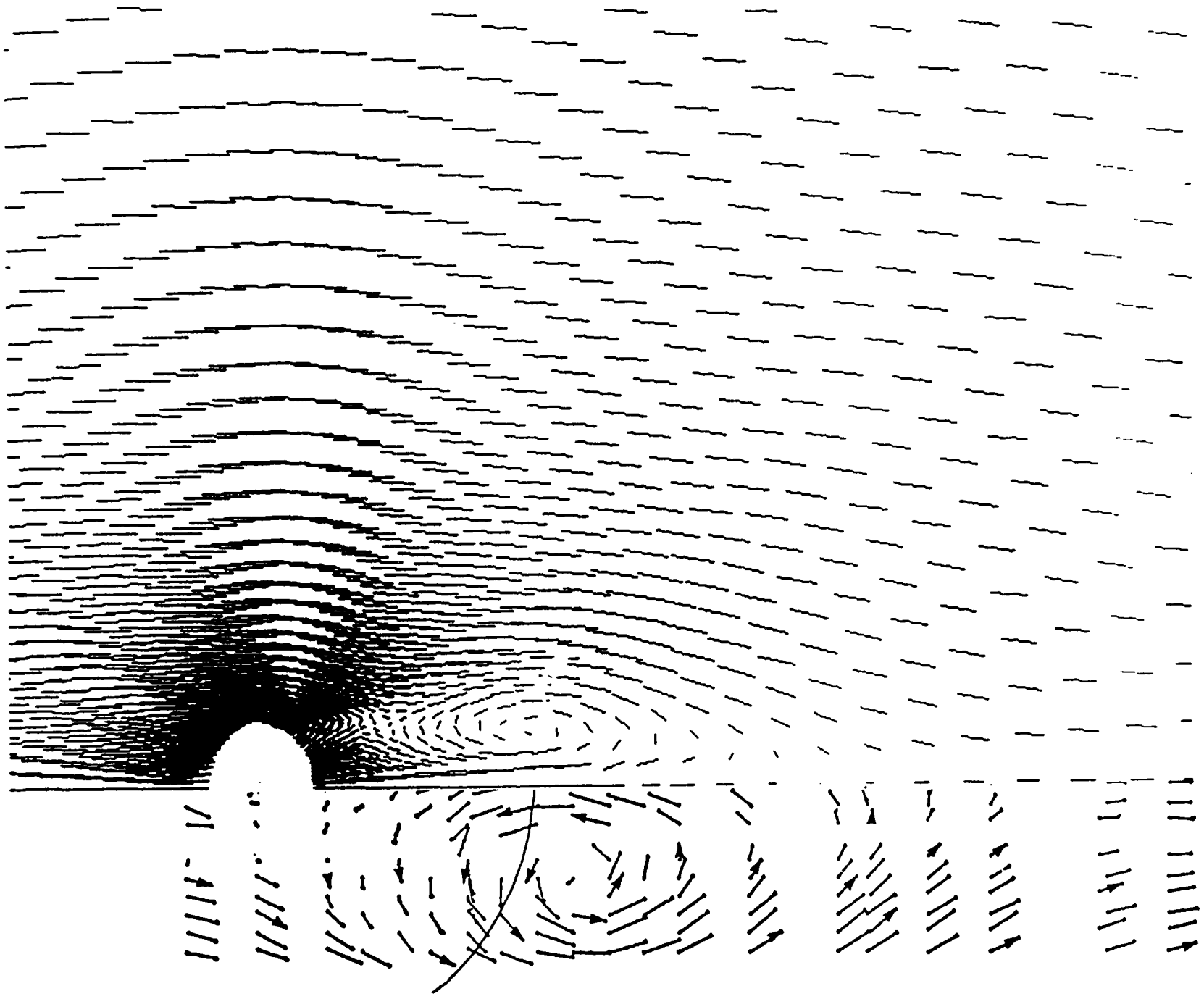

Figure 7. Comparison of Computed and Measured Transverse Velocity Field.

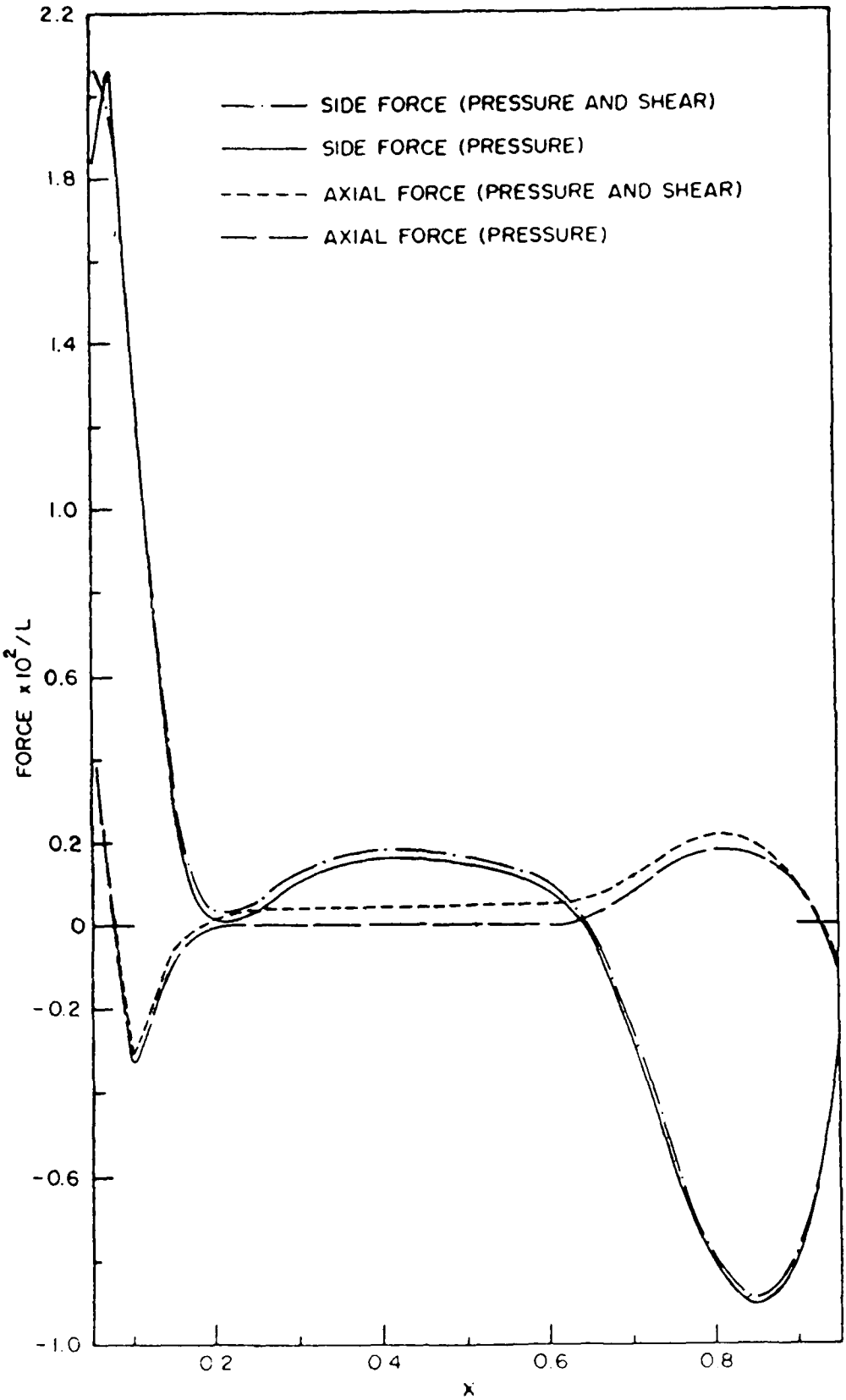

Figure 8. Computed Axial and Side Force Distributions.